An Eulerian-Lagrangian method for simulating the interaction of a Non-Newtonian fluid with complex shaped micro-swimmers

B. Vargas-Torres, T. Solano, Y. Liu, K. Shoele, H. Mohammadigoushki, M. Sussman

March 17, 2022

I Method

The numerical method used for the Eulerian part of our micro-swimmer simulations is a staggared grid, dynamic adaptive mesh refinement algorithm for incompressible multiphase flow. The dynamics of the micro-swimmer geometry, represented on a Lagrangian grid, is coupled to the Eulerian fluid flow by way of converting the Lagrangian representation of the micro-swimmer to a Moment-of-Fluid Eulerian representation. The details of the numerical method are presented in the following journal articles: [1, 3, 5, 6].

It is important to note that my results correspond to a staggared grid formulation which is known to have better stability properties than the collocated formulation [8]. The source of the stability problems for a collocated grid algorithm is that the pressure projection step corresponding to the collocated formulation has a non-empty null space in the pattern of a checkerboard velocity distribution.

The numerical algorithm for simulating non-Newtonian multi-fluid/multi-phase flows that was presented in [5] was for a collocated grid. The numerical algorithm presented in [6] was for a staggared grid, but only Newtonian flows were simulated in [6]. The non-Newtonian multi-fluid/multi-phase results presented in this report are distinct from [5] in that the present results were computed on a staggared grid.

The potential pitfalls of the collocated formulation notwithstanding, in Figures 1, 2, and 3 below, it is observed that the collocated results of the past agree, qualitatively, with the present staggared grid results. This is encouraging, since the present results (a) reinforce that the previous reported collocated results were valid and did not suffer from stability problems, and (b) reinforce that the present staggared grid method has been implemented correctly, and has a mathematical guarantee of stability [4] for future simulations.

The mathematical model governing our numerical method is given as follows:

$$\nabla \cdot \vec{u} = 0 \tag{1}$$

$$\frac{\partial(\rho\vec{u})}{\partial t} + \nabla \cdot (\rho\vec{u}\vec{u}^T) = \nabla \cdot (-p\boldsymbol{I} + \boldsymbol{\tau}) \tag{2}$$

$$\boldsymbol{\tau} = \boldsymbol{\tau}_s + \boldsymbol{\tau}_p \tag{3}$$

$$\boldsymbol{\tau}_s = 2\mu_s \boldsymbol{D} = \mu_s(\nabla\vec{u} + \nabla\vec{u}^T) \tag{4}$$

$$\boldsymbol{\tau}_p = \frac{\mu_p \boldsymbol{f} s(\boldsymbol{A})}{\lambda} \tag{5}$$

$$\overset{\triangledown}{\boldsymbol{A}} \equiv \frac{\partial \boldsymbol{A}}{\partial t} + \nabla \cdot (\vec{u}\boldsymbol{A}) - \boldsymbol{A} \cdot \nabla\vec{u} - (\nabla\vec{u})^T \cdot \boldsymbol{A} = -\frac{f_R(\boldsymbol{A})}{\lambda} \tag{6}$$

$$\frac{\partial \phi_m}{\partial t} + \vec{u} \cdot \nabla\phi_m = 0 \quad m = 1, \ldots, M \tag{7}$$

$\vec{u}$ is the fluid velocity, ρ is the density which can have large jumps at material interfaces, p is the pressure, and $\boldsymbol{\tau}$ is a combination of the solvent stress tensor $\boldsymbol{\tau}_s$ and polymer stress tensor, $\boldsymbol{\tau}_p$. μ_s is the solvent viscosity

which can have large jumps at material interfaces, $\boldsymbol{D}$ is the rate of deformation tensor, $bmD = \nabla\vec{u} + \nabla\vec{u}^T)$, and $\boldsymbol{A}$ is the configuration tensor. ϕ_m is the level set function for material m ($m = 1, \ldots, M$) and satisfies,

$$\phi_m(t,\vec{x}) = \begin{cases} +d_m & \text{if } \vec{x} \text{ is in material } m \text{ at time } t \\ -d_m & \text{if } \vec{x} \text{ is not in material } m \text{ at time } t. \end{cases} \tag{8}$$

d_m in (8) represents the closest distance from point $\vec{x}$ to the material m interface. The relaxation source term $f_R(\boldsymbol{A})$ found in (6) is defined as follows

$$f_R(\boldsymbol{A}) = \begin{cases} \frac{\boldsymbol{A}}{1-\mathrm{tr}(\boldsymbol{A})/L^2} - \boldsymbol{I} & \text{FENE-P model} \\ \frac{\boldsymbol{A}-\boldsymbol{I}}{1-\mathrm{tr}(\boldsymbol{A})/L^2} & \text{FENE-CR model} \end{cases} \tag{9}$$

The polymer stress versus strain term $f_s(\boldsymbol{A})$ found in (5) is defined as follows

$$f_s(\boldsymbol{A}) = \begin{cases} \frac{\boldsymbol{A}}{1-\mathrm{tr}(\boldsymbol{A})/L^2} - \boldsymbol{I} & \text{FENE-P model} \\ \frac{\boldsymbol{A}-\boldsymbol{I}}{1-\mathrm{tr}(\boldsymbol{A})/L^2} & \text{FENE-CR model} \end{cases} \tag{10}$$

We refer the reader to the following references for more information on the mathematical models for non-Newtonian fluids [2, 7].

The (novel) results presented in this report are preliminary in that we only present results for the one-way coupling between the swimmer (prescribed Lagrangian description of its motion) and the non-Newtonian fluid (Eulerian description of its motion). The prescribed swimmer motion influences the fluid motion but the fluid motion does not in turn effect the swimmer motion. The swimmer (see Figures 2 and 3) undergoes rigid body motion in the form of translation along the z axis, $\vec{u}_{translate} = (0, 0, w)$ and rotation about the z axis $\vec{u}_{rotate} = (-\Omega y, \Omega x, 0)$:

$$\frac{d\vec{x}_{swimmer}}{dt} = \vec{u}_{translate} + \vec{u}_{rotate}. \tag{11}$$

The Eulerian fluid motion is coupled to the prescribed Lagrangian swimmer motion by way of the no-slip condition,

$$\vec{u}_{fluid}(t,\vec{x}) = \vec{u}_{translate}(\vec{x}) + \vec{u}_{rotate}, \tag{12}$$

which is satisfied by all points $\vec{x}$ on the swimmer surface at time t.

II Results

Two types of results are presented in this report: (A) verification results, and (B) validation results.

II.1 Verification Results: Rising gas bubble in non-Newtonian fluid

In Figure 1 we compare computational results for the rise of a gas bubble in a hybrid shear thinning and FENE-CR liquid solution [5]. The model parameters for this test correspond to the parameters used in [5] (see Figure 7 from [5]). The viscoelastic model is the hybrid Shear thinning Carreau and FENE-CR model. The specific non-Newtonian model parameters are $n = 1/2$, $L = 10$, and $De = 5$. We expect to compute a bubble that attains a very unique "cusped-cap" shape.

In our Figure 1, we show the following 3 results: (a) collocated results from [5], (b) staggared quarter domain 3D resuts (mirrored across the $x - z$ and $y - z$ planes for comparison purposes) computed using our latest algorithm, and (c) staggared 3D RZ (axisymmetric R-Z) results (revolved about the z axis for comparison purposes).

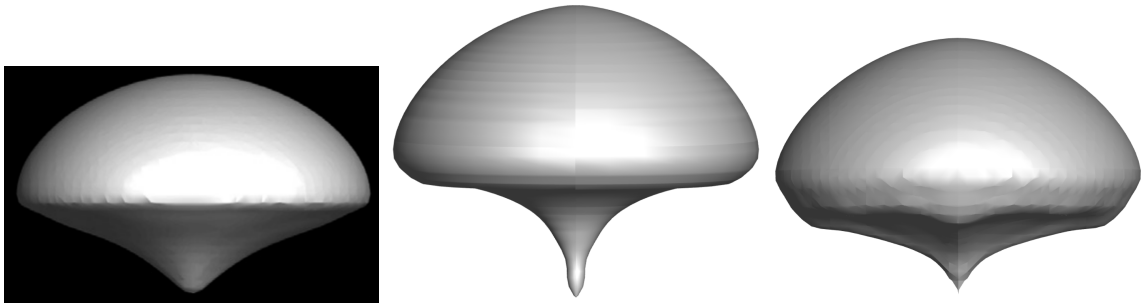

Figure 1: Comparison between staggared and unstaggared algorithms for a gas bubble rising in a non-newtonian fluid; from left to right: (a) collocated results 3D, (b) staggared results, 3D axi-symmetric, at time $t = 0.434$, (c) staggared results, 3D, quarter domain simulation at time $t = 0.472$.

II.2 Validation Results: Helical swimmer in non-Newtonian fluid

In Figures 2 and 3 we compare previous results for the Q_{11} component of the configuration tensor using the collocated algorithm with the current staggared grid algorithm. The pitch angle in Figure 2 is 12.4 degress and the pitch angle in Figure 3 is 47.5 degrees. The liquid surrounding the swimmer is modeled as a FENE-P fluid. The translational motion for both staggared grid simulations was 0.00355 cm/s. Unfortunately, after the simulations were completed, it was discovered that the translational motion for the 12.4 collocated case was 0.015 cm/s and the translational motion for the 47.5 collocated case was 0.027cm/s.

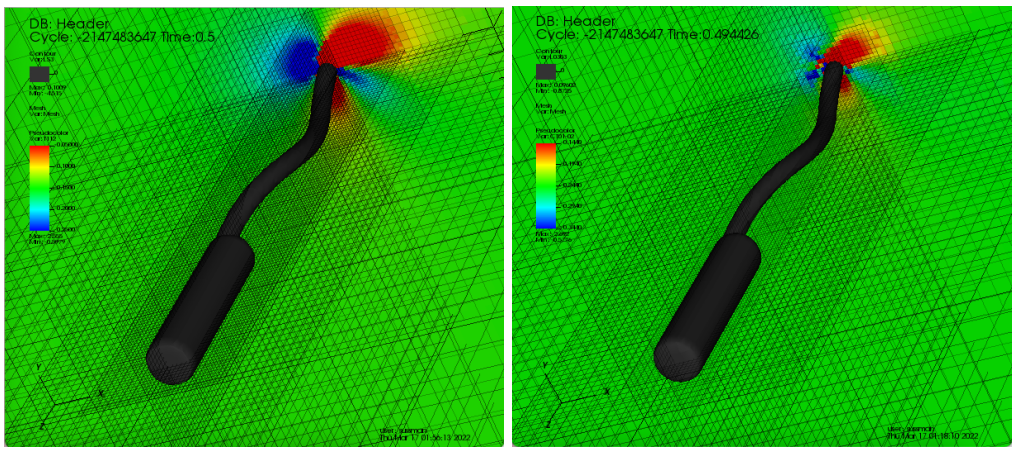

Figure 2: Comparison (Q_{11} component) between staggared and unstaggared algorithms for non-Newtonian FENE-P flow past a helical swimmer with pitch angle $12p4$ degrees. (a) left: collocated results, (b) right: staggared results, at time $t = 0.5$.

III Conclusions

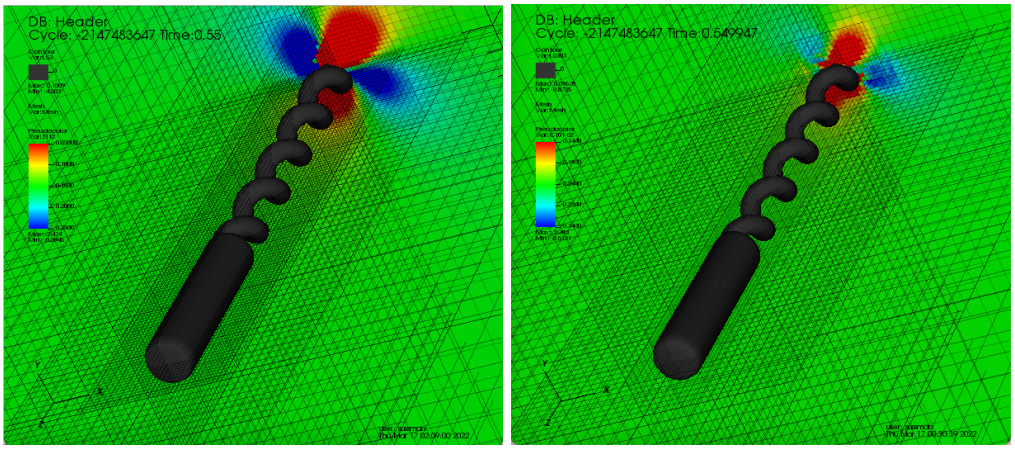

Figure 3: Comparison (Q_{11} component) between staggared and unstaggared algorithms for non-Newtonian FENE-P flow past a helical swimmer with pitch angle 47.5 degrees. (a) left: collocated results, (b) right: staggared results, at time $t = 0.55$.

References

[1] Arienti, M., and Sussman, M. An embedded level set method for sharp-interface multiphase simulations of diesel injectors. *International Journal of Multiphase Flow 59* (2014), 1–14.

[2] Bird, R., Dotson, P., and Johnson, N. Polymer solution rheology based on a finitely extensible bead—spring chain model. *Journal of Non-Newtonian Fluid Mechanics 7*, 2 (1980), 213–235.

[3] Dyadechko, V., and Shashkov, M. Moment-of-fluid interface reconstruction. *Los Alamos report LA-UR-05-7571* (2005).

[4] Guittet, A., Theillard, M., and Gibou, F. A stable projection method for the incompressible navier–stokes equations on arbitrary geometries and adaptive quad/octrees. *Journal of Computational Physics 292* (2015), 215–238.

[5] Ohta, M., Furukawa, T., Yoshida, Y., and Sussman, M. A three-dimensional numerical study on the dynamics and deformation of a bubble rising in a hybrid carreau and fene-cr modeled polymeric liquid. *Journal of Non-Newtonian Fluid Mechanics 265* (2019), 66–78.

[6] Pei, C., Vahab, M., Sussman, M., and Hussaini, M. Y. A hierarchical space-time spectral element and moment-of-fluid method for improved capturing of vortical structures in incompressible multiphase/multi-material flows. *Journal of Scientific Computing 81*, 3 (2019), 1527–1566.

[7] Purnode, B., and Crochet, M. Polymer solution characterization with the fene-p model. *Journal of Non-Newtonian Fluid Mechanics 77*, 1 (1998), 1–20.

[8] Rhie, C. M., and Chow, W.-L. Numerical study of the turbulent flow past an airfoil with trailing edge separation. *AIAA journal 21*, 11 (1983), 1525–1532.